Design of an efficient thulium-doped fiber amplifier for dual-hop earth to satellite optical wireless links

Jawad Mirza [a], Ahmad Atieh [b], Muhammad Ilyas Menhas [c], Salman Ghafoor [d], Musab Magam [e], Laiq Jamal [e], Sharif Iqbal Mitu Sheikh [f], Khurram Karim Qureshi [f,*]

[a] SEECS Photonics Research Group, Islamabad, Pakistan
[b] Optiwave Systems Inc., Ottawa, Ontario, Canada
[c] Department of Electrical Engineering, Mirpur University of Science and Technology, Mirpur, AJK, Pakistan
[d] SEECS, National University of Sciences and Technology, Islamabad, Pakistan
[e] Department of Electrical Engineering, King Fahd University of Petroleum and Minerals, Saudi Arabia
[f] Department of Electrical Engineering and Center for Communication Systems and Sensing, King Fahd University of Petroleum and Minerals, Saudi Arabia

ARTICLE INFO

ABSTRACT

Optical wireless communication (OWC) links enable high-speed data transmission between earth stations and satellites. The propagation of optical signals through the atmosphere suffer from atmospheric attenuation and turbulence due to rain, fog, snow, clouds, and wind. The impact of these impairments on propagation of optical signals becomes more pronounced in the case of deep space links. Therefore, optical amplifiers of high output power and gain are extremely useful in deep space links to achieve error free transmission by improving the link budget. In this paper, we propose the design of an efficient Thulium-doped fiber amplifier (TDFA) as booster as well as an in-line based on dual-stage pumping scheme for employment in a dual-hop earth to satellite OWC Link. The pumping scheme, length of Thulium-doped fiber (TDF), and Tm^{3+} concentration in the proposed design of TDFA are optimized in such a way so that high output power and gain are achieved for booster and in-line stages, respectively. Output power and gain of 4.6 W and 18.8 dB, respectively are achieved for signal power of 0 dBm at 1807.143 nm when TDFA is used as booster amplifier. Similarly, gain and output power of 66.6 dB and 1.5 W, respectively are achieved for signal power of −35 dBm at 1807.143 nm when TDFA is used as in-line amplifier. A noise figure (NF) of 4.4 dB is achieved for signal wavelength of 1807.143 nm and power of 0 dBm. Finally, the system level performance of the designed TDFA is investigated using bit error rate (BER) metric for a dual-hop earth to satellite OWC wavelength division multiplexed (WDM) transmission system of four quadrature phase shift keying (QPSK) modulated optical signals with an aggregate data rate of 104 Gbps. The BER results showed different possible ranges of error-free transmission at the forward error correction (FEC) limit of 10^{-4} for different values of atmospheric attenuation.

© 2022 THE AUTHORS. Published by Elsevier BV on behalf of Faculty of Engineering, Ain Shams University. This is an open access article under the CC BY-NC-ND license (http://creativecommons.org/licenses/by-nc-nd/4.0/).

1. Introduction

The rapid progress in development of low attenuation around 1550 nm silica based single mode fibers (SMFs), Erbium-doped fiber amplifiers (EDFAs), wavelength division multiplexing (WDM), and newly introduced digital coherent transmission have taken the internet infrastructure at its climax. Hence, record transmission speed and capacity of 1.6 Tb/s by wavelength division multiplexing of 160 optical channels over a single SMF was demonstrated recently [1]. Due to inception of various technologies in our daily life such as IoTs, HDTVs, high-definition online streaming, video gaming, video conferencing, social media platforms, VoIP

Production and hosting by Elsevier

J. Mirza, A. Atieh, M.I. Menhas et al.

etc result into a rapid increase in internet traffic [2,3]. Telecom networks today are swiftly being pushed towards their capacity limits as a result of customers demand for high-speed and high-data rate transmission to run the bandwidth intensive services and applications. Hence, the network designers and telecom operators have forseen a future "capacity crunch" [4]. Therefore, the fibre-optic transmission systems based on most favourite and currently exhausted 1550 nm optical window is supplemented by the introduction of new optical windows to contain the rapid increase in demand for greater bandwidth [2,5]. Different solutions have been considered by the research community to address the capacity and bandwidth demand related problems of fibre-optic transmission systems. For example, (I) optimal use of the available limited resources by employing advance multi-level modulation formats such as PAM-4/8, 64-QAM etc, (II) development of the communication systems based on multi-mode fibers (MMFs) to accommodate more spatial data streams, and (III) development of the efficient multi-band transmission (MBT) systems based on exploiting the theoratically unlimited bandwidth of the existing silica SMFs [6]. The MBT systems rely upon the design and development of novel active and passive optical components and use of existing infrastructure for the efficient transmission in O-, E-, S-, L-, U-bands, and beyond [7]. Therefore optical window around 1900 nm is getting huge research attraction for future optical communication systems as an extension to the C-, L-, and U-bands.

The growing research interests around 1900 nm optical window are compelling to find optical amplifiers that provide high gain, high saturated output power, and low NF. TDFAs enable significantly enhanced amplification bandwidth by operating in 1750–1950 nm wavelength range and have attracted huge research attractions for potential applications such as optical communication, spectroscopy, remote sensing, photo-medicine, material processing, and mid-IR generation [4,8,9]. Due to recent boom in research interests in optical communication window around 1900 nm, TDFAs are being widely explored in near past. R. E. Tench et al. demonstrated a dual-stage 940 nm multimode semiconductor pumped polarization maintaining TDFA (PM-TDFA) with a high output power of 2.2 W and gain over 46 dB at 1909 nm. Wide operating bandwidth of 1875–2000 nm and NF of 7 dB was observed [8]. Romano et al. reported performance evaluation of a dual-stage single clad TDFA of high output power and gain of 5 W and 60 dB at 1952 nm without stimulated Brillouin scattering (SBS). A power conversion efficiency (PCE) over 60% was achieved [10]. Muravyev et al. demonstrated [11] an ultrabroadband TDFA promising the gain of 30 dB and 7 dB simultaneously at 1900 nm and 2300 nm, respectively in a Tm^{3+}-doped tellurite fiber. C. Gaida et al. proposed a TDFA of record average output power of 1 kW pumped with state-of-the-art laser diodes of combined pump power of around 2 kW at 793 nm [12]. PCE of more than 60% has been achieved. Mukhatar et al. theoretically analyzed the performance of an in-band pumped TDFA operating at 1900 nm [13]. The performance is analyzed by considering the optimized doping concentration of Tm^{3+}, TDF length, and the pump power. A small-signal gain of around 41 dB is demonstrated at optimized parameters. The minimum NF of 4.15 dB is observed at 1900 nm. X. Jin et al. demonstrated a high-efficiency ultrafast TDFA based on a resonant pumping technique by employing a CW fiber laser at 1940 nm as pump source [14]. Maximum output power of 40 W and PCE of 87% was observed at 1970 nm when the launched pump power was 53 W. The performance of a heavily doped TDFA has been theoretically investigated for operating at 2000 nm when pumped at 1570 nm with power of 2 W in [15]. Small-signal gain of 35 dB was achieved at optimum TDF length of 0.7 m. Khamis et al. investigated the dynamic behavior of a TDFA operating at 2000 nm for 20 channels having −4 dBm total input power reconfigurable WDM system [16]. It has been shown by simulation

results that the deleterious channel power fluctuations which are generated by variation in signal power can be mitigated by proposed optical gain-clamping technique. In [17], the short wavelength amplification in 1650–1800 nm wavelength range is investigated using silica-based TDFAs. A gain of around 29 dB was demonstrated by in-band diode pumped TDFA operating in 1650–1800 nm wavelength range and NF as low as 6.5 dB was observed. M. A. Khamis et al. proposed a theoretical model of TDFA by considering the cross-relaxation process and different pump wavelengths [18]. It has been shown that the performance of TDFA is more better for 1570 nm pump instead of 793 nm pump. Therefore, peak gain of 30 dB was achived for pump and signal powers of 27 dBm and −10 dBm, respectively for signal wavelength of 1840 nm is used while only 22 dB gain was achieved using indirect pumping at 793 nm under the same conditions. Jung et al. proposed several designs of silica-based in-band pumped at 1550 nm TDFAs operating across the 1650–2050 nm wavelength range [19]. A broadband gain of 36 dB, NF of 4.5 dB, and saturated output power of 100 mW over 400 nm were demonstrated by using these designs of TDFA for short, central, and long wavelength operation. A multiwatt dual-stage TDFA employing a 1567 nm L-band shared pump source was experimentally demonstrated in [20]. The performance of the TDFA was evaluated for three specific signal wavelengths of 1909 nm, 1952 nm, and 2004 nm. High gain, output power, and NF of 60 dB, 2 W, and 4 dB, respectively were observed. In [21], a TDFA model was proposed to study various performance characteristics such as peak temperatures, expected output powers and efficiencies, presence of amplified spontaneous emission (ASE), and transverse mode instability (TMI) by considering single as well as two-tone configurations based on numerical simulations. Singh et al. analyzed the gain performance of a S-band silica based TDFA by employing multiple pumping schemes [22]. The pumping schemes of 1050 nm, 1050 nm + 800 nm, 1050 nm + 1400 nm, and 1050 nm + 1400 nm + 800 nm have been considered. It has been demonstrated that the best gain enhancement was achieved for 1050 nm + 1400 nm + 800 nm pumping combinition. R. E. Tench et al. demonstrated through experimental and simulation results a tandem single clad TDFA operating in 1900–2050 nm wavelength range which was in-band pumped at 1560 nm [23]. High gain > 50 dB, output power of 2.6 W, dynamic range >30 dB, and NF around 4 dB were achieved. R. E. Tench et al. reported the design of a broadband hybrid single-clad PM-HDFA/TDFA operating in 2000–2100 nm wavelength range [24]. Small-signal gain of 49.1 dB, NF of 6.5 dB, and output power of 3.54 W were achieved at signal wavelength of 2051 nm. R. E. Tench et al. reported the design of a broadband hybrid PM-HTDFA operating in 2000–2100 nm wavelength range [25] generating an output power of over 25 W at 2051 nm and a dynamic range of 34 dB. We compare the main structural artifacts and results obtained from the proposed design (in bold) with published work as reported in the literature. It may be observed from Table 1 that the proposed design of TDFA gives good performance along with added advantages of simplicity and cost efficiency. It is also worth mentioning here that the past studies mentioned in Table 1 are mainly experimental which may not be directly compared with our work, which is simulation based. However, our work paves the way for research groups having relevant facilities to perform experimental investigations. In this work, we propose the design of an efficient TDFA operating in 1700–1950 nm wavelength range employing a dual-stage pumping technique at 1210 nm with two forward pump sources each of 2.5 W. The pumping scheme, TDF length, and doping concentration of Tm^{3+} are optimized to achieve high output power and gain for the use in dual-hop earth to satellite OWC links as booster as well as in-line amplifier, respectively. Output power and gain of 4.6 W and 18.8 dB are achieved in the case of TDFA as booster amplifier while gain and output power of

Table 1
Comparison of the important results of the proposed work with results of the past related studies.

Study	Gain	NF	PCE	TDF length	No. of pumps & pumping stages
[8]	46 dB	7 dB	26.5%	4 m, 2 m	1, 2
[10]	60 dB	7 dB	78.7%	4.3 m, 2 m	2, 2
[12]	-	-	60%	-	2, 1
[13]	41 dB	4.2 dB	-	10 m	1, 1
[14]	-	-	87%	7 m	2, 1
[15]	35 dB	-	-	0.7 m	1, 1
[17]	29 dB	6.5 dB	-	0.5 m, 0.5 m	2, 1
[18]	30 dB	6.5 dB	-	1.25 m	2, 1
[19]	36 dB	4.5 dB	-	8 m	2, 1
[20]	60 dB	4 dB	54.2%	4.3 m, 2 m	1, 2
[22]	27 dB	6.5 dB	-	10 m	3, 1
[23]	50 dB	4 dB	82%	7 m, 5 m	3, 2
[24]	49.1 dB	6.5 dB	13.4%	3 m, 2.5 m	1, 2
[25]	54 dB	10 dB	70%	3 m, 2 m, 5 m	3, 3
[Proposed]	**66.6 dB**	**4.4 dB**	**95%**	**1.5 m, 1.5 m**	**2, 2**

66.6 dB and 1.5 W are achieved in the case of TDFA as in-line amplifier for signal power of 0 dBm and −35 dBm, respectively at 1807.143 nm. NF of around 4.4 dB is observed for signal wavelength of 1807.143 nm and power of 0 dBm. The system level performance of the TDFA is investigated for a dual-hop earth to satellite OWC link by considering WDM transmission of four QPSK modulated optical signals having an aggregate data rate of 104 Gbps. The BER performance metric is used for different atmospheric attenuation while considering strong turbulence regime (refractive index structure parameter of $5 \times 10^{-12} m^{-2/3}$) using Gamma-Gamma channel model for OWC link.

We implemented the proposed design using a well known optical communication system design software "OptiSystem" from Optiwave System Inc [26]. The software is used to optimize the pumping scheme, length of TDF, and Tm^{3+} concentration. The system level performance of the TDFA is analyzed by considering Gamma-Gamma channel model.

2. Application Scenario of the Proposed TDFA

Satellite communications have been getting rapid attention in variety of applications where terrestrial communication networks usually flop in meeting a particular requirement, such as remote sensing, earth observatory, military surveillance, radio astronomy, deep space exploration, broadband backhaul communication, satellite constellation, and navigation [27]. These applications require the transmission of huge amount of data, i. e in Tb/s from earth to satellite, satellite to earth, satellite to satellite, satellite to airborne platforms etc. It is predicted that the data volume will surpass 7 PB/year in the near future [28]. Consequently, the traditional X to Ka satellite frequency bands being used for data transmission are expected to reach their capacity limit soon [28]. OWC is the latest technology in which high power laser beams either in the visible or infrared range are used to transfer the information from one point to another using a pair of telescopes through an unguided channel which may be in the atmosphere, free space or both [29,30]. OWC systems offer very high data rates comparable to optical fibers, easy installation, unlicensed spectrum utilization, low power consumption, low carbon footprint, compact, and highly secure to eavesdroppers [29,31]. Therefore, the use of OWC links in satellite communication is a viable solution. However, OWC links are also vulnerable to various detrimental effects arising from unstable weather conditions and geometry of telescopes [32]. The major impairments which affect the quality of service in OWC links are atmospheric attenuation, turbulence, and pointing errors [32] which limit the range of OWC links by compromising

the link budget. One of the solutions to extend the range of the OWC links is the transmission of high power optical signals by using high power lasers and booster amplifiers at the transmitters to maintain sufficient link budget [33]. Alternatively, use of relay assisted OWC techniques based on all-optical amplify and forward (OAF) or all-optical regenerate and forward (ORF) relays help in realizing the long range OWC links by combatting the above mentioned impairments [33]. As mentioned earlier that atmospheric attenuation, turbulence, and pointing errors limit the range of OWC links due to insufficient link budget. Therefore, the earth stations are usually equipped with high power laser sources and booster amplifiers to transmit the high power laser beams through free space in order to compensate the atmospheric attenuation and pointing errors so that sufficient link budget can be maintained. Different weather conditions can cause variable extent of atmospheric attenuation and turbulence. Normally, all weather related disturbances occur inside of the troposphere, which extends up to an altitude of 11 km [34]. Therefore, the influence of the atmosphere on OWC link beyond 11 km altitude up to geostationary earth orbit (GEO) is much smaller than it is for an OWC link from earth station to upper boundry of the troposphere. It is estimated that the atmospheric attenuation from an altitude of 11 km towards GEO is around 0.22 dB for a wavelength of 1550 nm [34]. It is also inferred that the loss will be even much smaller for longer wavelength beyond 1550 nm. Fig. 1 shows the application scenario of the proposed design of TDFA for employment in a dual-hop earth to satellite OWC link. It may be observed that an earth station is installed on surface of the earth and equipped with high power TDFA as booster amplifier. After power boosting, the earth station transmits the data modulated optical signal over OWC link using a telescope towards a high-altitude platform station (HAPS) which is at an altitude of 10 km above earth surface as shown in Fig. 1. As the OWC link between earth station and HAPS is more significant for weather related disturbances, therefore the high output power TDFA is used at earth station to efficiently encounter the atmospheric attenuation. The optical signal is then received at HAPS with the help of a telescope. The HAPS functions here as an OAF relay which houses the high gain TDFA as in-line amplifier. As the OWC link beyond troposphere is not significant for weather related disturbances, therefore the prime requirement here is the improvement of the gain instead of power boosting. Therefore, high gain TDFA is used at HAPS to improve the signal quality. After amplification, the optical signal is then transmitted over OWC link towards low earth orbit (LEO) satellite where the signal is received and further processed. A LEO is relatively close to earth's surface. It is normally at an altitude of less than 1000 km but could be as low as 200 km above the earth [34].
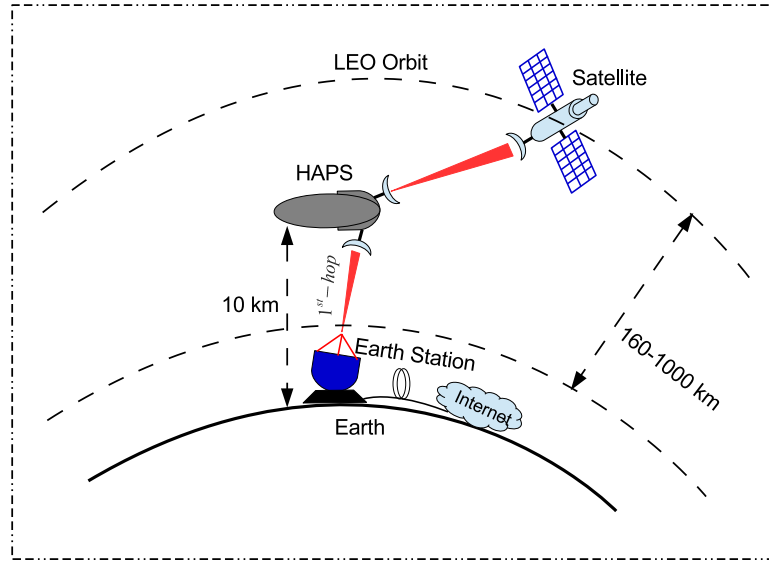
Fig. 1. Application scenario of the proposed design, **HAPS**: High-altitude platform station, **LEO**: Low earth orbit.

3. Theoretical Background

Fig. 2a shows the absorption and emission spectra of Tm^{3+}. It may be observed that although Tm^{3+} has multiple pump absorption bands resulting into emission at different wavelengths but pumping around 793 nm, 1000 nm, 1064 nm, 1200 nm, 1400 nm, 1570 nm, 1600 nm, and 1840 nm is widely employed. In this work, 1210 nm pumps are used for pumping the TDFs in both of the stages. Fig. 2b shows the energy level diagram of Tm^{3+} where $^3H_6$ is taken as ground energy state and $^3H_4$ is the first excited manifold. The most common transition causing the lasing around 1800 nm is $^3H_6 \leftrightarrow {}^3H_4$. Similarly, the rate equations can be written as [35].

$$\frac{dN_1}{dt} = -\left(W_{10} + \frac{P_p\sigma_{ap}}{hf_p} + \frac{P_s\sigma_{as}}{hf_s}\right)N_1 + W_{21}N_2 + \frac{P_s\sigma_{as}}{hf_s}N_3 \quad (1)$$

$$\frac{dN_3}{dt} = \frac{P_s\sigma_{as}}{hf_s}N_1 - \left(W_{30} + \frac{P_p\sigma_{ap}}{hf_p} + \frac{P_s\sigma_{as}}{hf_s}\right)N_3 + W_{43}N_4 \quad (2)$$

$$\frac{dN_5}{dt} = \frac{P_p\sigma_{ap}}{hf_p}N_3 + (W_{50} + W_{52})N_5 \quad (3)$$

Neglecting the ASE and fiber attenuation, the propagation equations of pump and signal along the TDF in the z-direction can be written as [35].

$$\frac{dP_p}{dz} = -\Gamma_p(\sigma_{ap}N_0 - \sigma_{ap}N_1 - \sigma_{ap}N_3)P_p(z) \quad (4)$$

$$\frac{dP_s}{dz} = -\Gamma_s(\sigma_{es}N_3 - \sigma_{as}N_1 - \sigma_{01}N_0)P_s(z) \quad (5)$$

Various symbols used in Eq. (1)–(5) are shown in Table 2.

4. Optimization of pumping scheme

Apart from length of TDF and Tm^{3+} concentration, the pumping scheme is a crucial design constraint which affect the overall performance (i.e. PCE) and cost of TDFAs. Therefore, it is important to select a suitable pumping configuration before optimizing rest of the parameters. Fig. 3 shows different pumping schemes used to pump Tm^{3+}. In this work, we optimize the pumping configuration with the help of PCE values obtained from the plots between pump power and output power measured with an optical power meter (OPM) attached at the output of TDF in each pumping configurations i.e., forward, bidirectional, and dual-stage. We have used
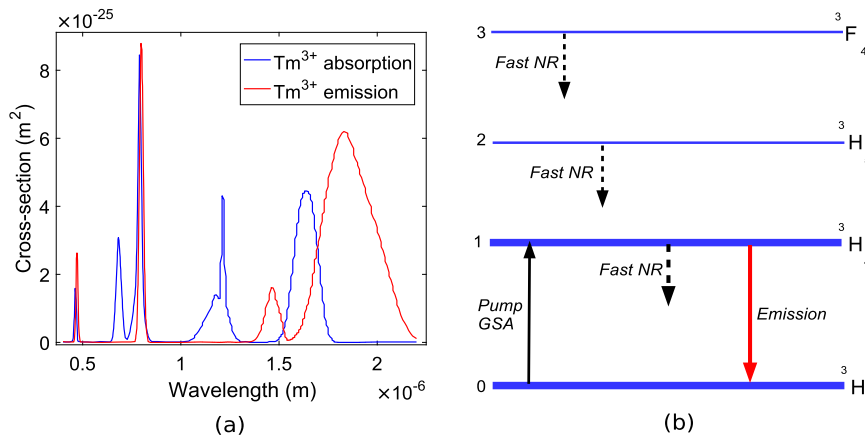

Fig. 2. (a) Absorption and emission spectra of Tm^{3+} (b) Energy level diagram of Tm^{3+}.

J. Mirza, A. Atieh, M.I. Menhas et al.

Table 2
Different symbols used in Eq. (1)–(5).

Sr. No	Symbol	Description
1	N_i	Population densities at i level
2	P_p, P_s	Pump and signal powers
3	hf_p, hf_s	Pump and signal photon energies
4	σ_{ap}, σ_{as}	Absorption cross-section of the pump and signal
5	σ_{es}	Emission cross-section of signal
6	σ_{01}	Transition cross-section from background leve to first excited level
7	Γ_p, Γ_s	Overlap integral of pump and signal
8	W_{ij}	Radiative transition rates from level i to level j
9	h	Plank's constant

same values of pump power, TDF length, and Tm^{3+} concentration in each configuration for a fair comparison. The Pumping scheme which produces the highest value of PCE will be considered as optimum pumping scheme. Fig. 4 shows pump power versus output power plots for different pumping configurations. The plot in the case of forward pumping configuration is obtained by considering the TDF length, Tm^{3+} concentration, signal power, and pump power of 3 m, $25 \times 10^{24} m^{-3}$, 0 dBm, and 5 W, respectively. Similarly, the plot in the case of bidirectional configuration is obtained by considering the TDF length, Tm^{3+} concentration, signal power, and pump power of 3 m, $25 \times 10^{24} m^{-3}$, 0 dBm, and 5 W (2.5 W for each pump), respectively. Finally, the plot in the case of dual-stage configuration is obtained by considering the TDF length, Tm^{3+} concentration, signal power, and pump power of 3 m (1.5 m for each TDF) [10], $12.5 \times 10^{24} m^{-3}$ for each TDF [10], 0 dBm, and 5 W (2.5 W for each pump) [10], respectively. The signal and pump wavelengths used in each configuration are 1807 nm and 1210 nm, respectively. It may be observed that forward, bidirectional, and dual-stage pumping configurations yield PCE of 41.7%, 39.6%, and 95% respectively. Therefore, it is concluded that dual-stage is the optimum pumping configuration which produces the highest PCE.

5. Simulation setup

The schematic of the proposed design of TDFA as booster as well as in-line amplifier based on dual-stage pumping has been shown in Fig. 3c. It is important to mention here that TDFs in this work are pumped using semiconductor laser diodes, but alternatively can be pumped using fiber laser based pump sources as we did in one of our past works [36]. Dual port WDM analyzer, OPM, and optical
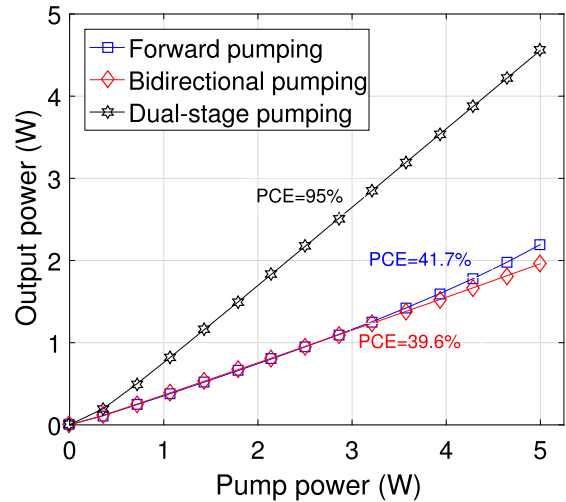

Fig. 4. Plots between pump power versus output power for different pumping configurations.

spectrum analyzer (OSA) are used to monitor and analyze the results.

The schematic of system level performance analysis of the designed TDFA as booster as well as in-line amplifier in a dual-hop earth to satellite OWC Link has been shown in Fig. 5. It may be observed that four CW signals having powers of 0 dBm and wavelengths of $\lambda_1 = 1800nm, \lambda_2 = 1800.8nm, \lambda_3 = 1801.6nm,$ and $\lambda_4 = 1802.4nm$ are modulated with electrical QPSK signals at the rate of 26 Gbps at earth station. The structure of optical QPSK transmitter is shown in inset of Fig. 5. The resulting optical QPSK signals are multiplexed and then the combined optical signal at an aggregate data rate of 104 Gbps is transmitted towards HAPS over first OWC link having range of 10 km after optical amplification with booster TDFA as shown in Fig. 5. The average optical power of combined signal at the input of transmitter telescope is 37 dBm. The signal is received at the HAPS where an in-line TDFA is installed. In other words, the HAPS simply plays the role of an OAF relay. After amplification, the average optical power of combined signal at the input of transmitter telescope is 31.5 dBm. The signal is then transmitted over second OWC link having range of 990 km towards LEO satellite. The power of the received optical signal by the receiver telescope is given by the following relation [37].
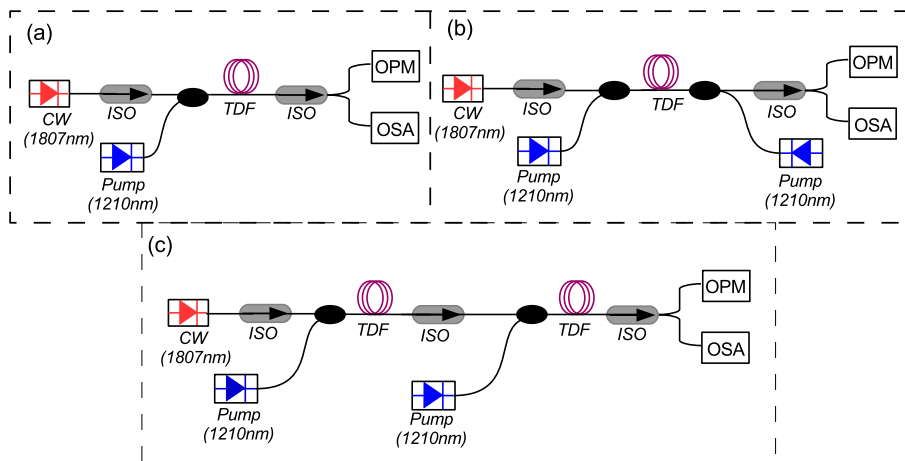

Fig. 3. Different pumping configurations for TDFA (a) Forward (b) Bidirectional (c) Dual-stage.
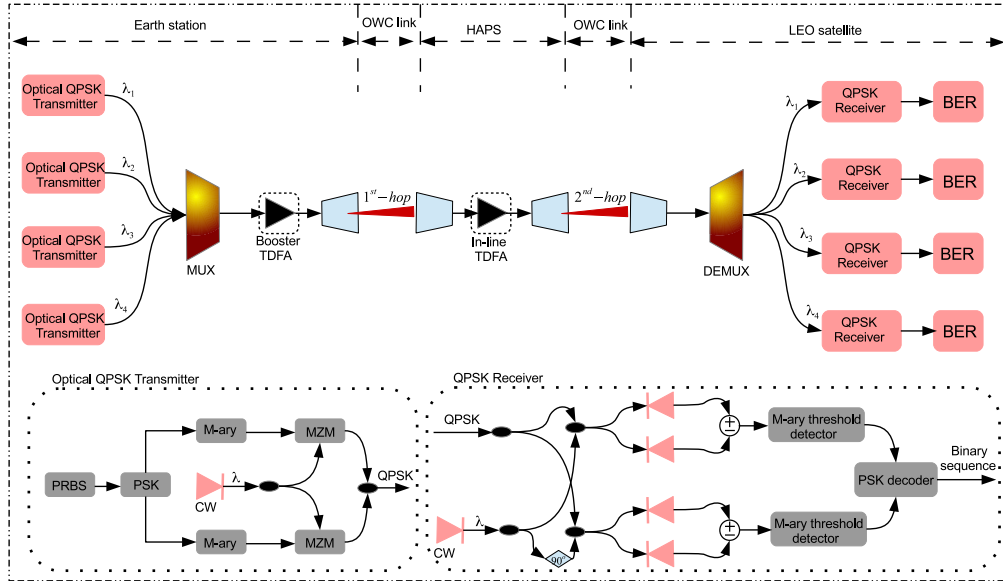
Fig. 5. Schematic of system level performance analysis of the designed TDFA.

$$P_r = P_t \eta_t \eta_r \left(\frac{\lambda}{4\pi L}\right)^2 G_t G_r L_t L_r \qquad (6)$$

Where; $P_t, P_r, \eta_t, \eta_r, \lambda$, L, G_t, G_r, L_t, and L_r is transmitted power, received power, transmitter optics efficiency, receiver optics efficiency, operating wavelength, length of OWC link, transmitter telescope gain, receiver telescope gain, transmitter pointing loss and receiver pointing loss, respectively. In Eq. 6, the receiver telescope gain is given by [37].

$$G_r = \left(\frac{\pi D_r}{\lambda}\right)^2 \qquad (7)$$

Where, D_r is the receiver telescope diameter. It may be observed from above expressions that the receiver telescope gain depends on receiver telescope diameter. Thus, smaller the telescope diameter, the less power received by it and vice versa. Both of the OWC links are modeled using Gamma-Gamma channel model [3]. The probability density function (PDF) of signal intensity fluctuations owing to atmospheric turbulence of OWC links is governed by Gamma-Gamma distribution which is given as [3,38].

$$p(I) = \frac{2(\alpha\beta)^{\frac{\alpha+\beta}{2}}}{\Gamma(\alpha)\Gamma(\beta)} I^{(\alpha+\beta)/2-1} K_{\alpha-\beta}\left(2\sqrt{\alpha\beta I}\right) \qquad (8)$$

Where, $K_n(.)$ is the Bessel function of nth-order and $\Gamma(.)$ is the Gamma function in terms of propagation distance z over OWC links as [38].

$$\Gamma(z) = \int_0^\infty exp(-t)t^{z-1}dt \qquad (9)$$

In the case of planar wave propagation, the parameters α and β representing large and small scale eddies of the scattering process, respectively are given by the following expressions [38].

$$\alpha = \left[exp\left(\frac{0.49\sigma_l^2}{(1+1.11\sigma_l^{2.4})^{1.17}}\right) - 1\right]^{-1} \qquad (10)$$

$$\beta = \left[exp\left(\frac{0.51\sigma_l^2}{(1+0.69\sigma_l^{2.4})^{0.833}}\right) - 1\right]^{-1} \qquad (11)$$

Where, $\sigma_l^2 = 1.23C_n^2k^{7/6}L^{11/6}$ is log intensity variance describing the strength of atmospheric turbulence, L is the length of OWC link in

km, $k = 2\pi/\lambda$ is the wave number, and C_n^2 is the refractive index structure parameter whose values can vary over time even for a specific link due to the complex dynamics of the weather. Normally, the value of C_n^2 varies from 10^{-17} for weak turbulence to 10^{-12} for strong turbulence [38]. After demultiplexing, the individual optical QPSK signals are detected by the QPSK receivers where optical to electrical conversion takes place based on the principle of homodyne detection. The structure of optical QPSK receiver is shown in inset of Fig. 5. After PSK decoding, the retrieved binary data signals are passed on to the BER test sets for BER calculation as shown in Fig. 5. The important simulation parameters used in this work are shown in Table 3.

6. Results and Discussion

This section discusses the design optimization of TDFA as booster as well as in-line amplifier and system level performance of the designed TDFA based on simulation results.

Table 3
Important simulation parameters.

Sr. No	Parameter	Value
1	Data rate (each channel)	26 Gbps
2	Range of first OWC link (first-hop) [34]	10 km
3	Range of second OWC link (second-hop) [34]	990 km
4	Atmospheric attenuation of first OWC link	5 dB/km
5	Atmospheric attenuation of second OWC link [34]	0.22 dB
6	Refractive index structure parameter (C_n^2) of both OWC links	$5 \times 10^{-12} m^{-2/3}$
7	Transmitter and receiver aperture diameter [39]	5 and 10 cm
8	Beam divergence	2 mrad
9	Pump wavelength	1210 nm
10	Pump power [10]	2.5 W
11	Core radius [35]	$1.3\mu m$
12	Numerical aperture [35,40]	0.3
13	Doping radius [41]	$1.3\mu m$
14	Signal attenuation	0.1 dB
15	Pump attenuation	0.15 dB
16	Responsivity of PIN	0.9 A/W
17	Temperature	300 K

6.1. TDFA as Booster Amplifier

The output power of the TDFA is calculated for different signal wavelengths at different lengths of the TDF and Tm^{3+} concentration with a signal power of 0 dBm and pumping powre of 5 W (2.5 W for each pump) as shown in Fig. 6. It may be observed from Fig. 6a that the output power of the TDFA is highest equals to 4.6 W at 1807.143 nm at 3 m length of TDF (1.5 m for each TDF) for Tm^{3+} concentration of $12.5 \times 10^{24} m^{-3}$ for each TDF. Hence, TDF length of 3 m is used as the optimum length which contributes towards maximum output power. Similarly, the plots between signal wavelength and output power are obtained at different Tm^{3+} concentrations by considering the optimized TDF length. It is obvious that the output power of TDFA is highest corresponding to Tm^{3+} concentration of $12.5 \times 10^{24} m^{-3}$ for each TDF as shown in Fig. 6b. The effect of TDF length and Tm^{3+} concentration on the particular shape of the plots shown in Fig. 6 is due to the amount of absorbed pump power and its conversion to higher wavelength to amplify the signal wavelength. The balance of the amount of absorption of the amplified signal and its gain due to pump conversion cause this particular shape of the plots.

Fig. 7 shows the plots between signal wavelength and gain as well as between signal wavelength and NF obtained at optimized parameters for a signal power of 0 dBm and pump power of 5 W (2.5 W for each pump). It may be observed from Fig. 7a that the maximum gain of 18.8 dB is obtained at 1807.143 nm. Similarly, Fig. 7b shows that NF of 4.44 dB is achieved at signal wavelength of 1807.143 nm, while a NF below 4.6 dB is achieved over 1700–1950 nm wavelength range. In order to study the impact of change in pump wavelength on output power and gain of TDFA, the pump wavelength is varied and its effect on output power and gain of

TDFA is observed by considering the optimized parameter for signal wavelength, pump power, and signal power of 1807.143 nm, 5 W (2.5 W for each pump), and 0 dBm respectively as shown in Fig. 8. It may be observed from Fig. 8a that the output power of TDFA decreases for 1190–1200 nm wavelength range and then it becomes almost constant for wavelengths longer than 1200 nm. The reason behind this trend can be understood considering the absorption and emission spectra of Tm^{3+} as shown in Fig. 2a. The Tm^{3+} has maximum absorption around 1210 nm, while at the same time absorbs part of the amplified signal as described in its absorption spectrum shown in Fig. 2a. However, the more the pump is absorbed, the higher gain the signal attains according to its emission spectra shown in Fig. 2a where a positive slope exists of interested amplified signal wavelength range. The balance between the absorption of the amplified signal and the amount of gain, the signal is amplified using the pump at a specific wavelength results in the behavior illustrated in Fig. 8a. Similarly, it may be noticed from Fig. 8b that the gain of the TDFA first increases gradually for 1190–1205 nm wavelength range. Beyond 1205 nm, a saturation region appears and the gain stops increasing significantly as evident from Fig. 8b. This trend may again be interpreted considering the absorption and emission spectra of Tm^{3+} as shown in Fig. 2a. It is clear that absorption of the pump photons gradually increases in 1190–1205 nm wavelength range with the peak absorption around 1210 nm, resulting in an increase in gain of the TDFA in this wavelength range. After 1210 nm, the absorption of the pump photons starts decreasing gradually which results into gain saturation. To validate the effect of pair-induced quenching (PIQ) on the output power and gain of the TDFA, the signal wavelength versus output power and gain plots are obtained by considering the effect of PIQ as shown in Fig. 9 at optimized parameters for pump and signal
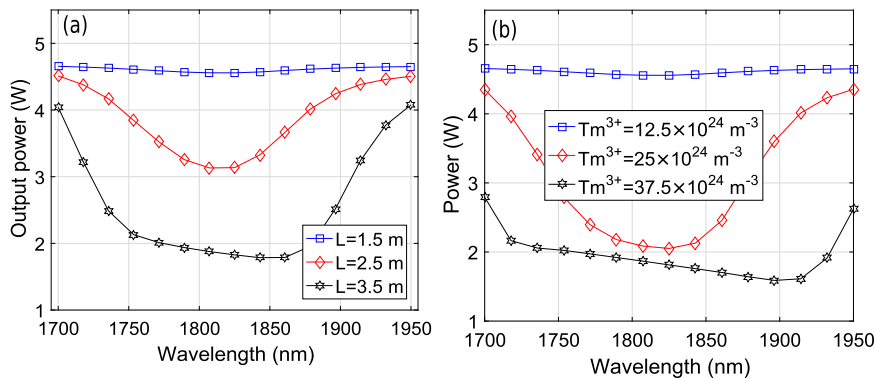

Fig. 6. Signal wavelength versus output power plots as a function of (a) TDF length (b) Tm^{3+} concentration.
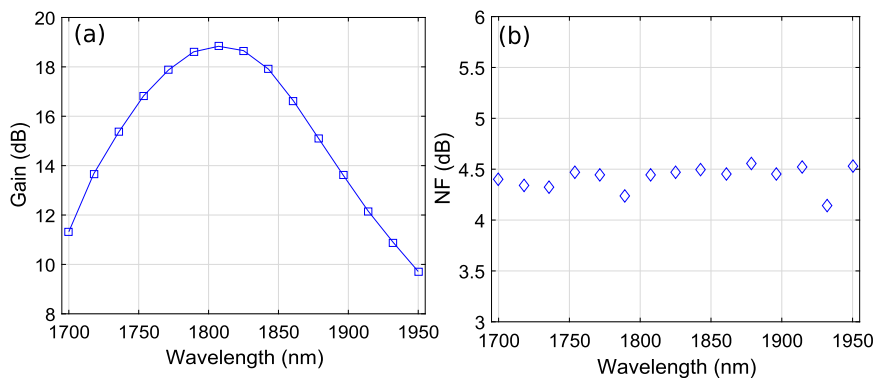

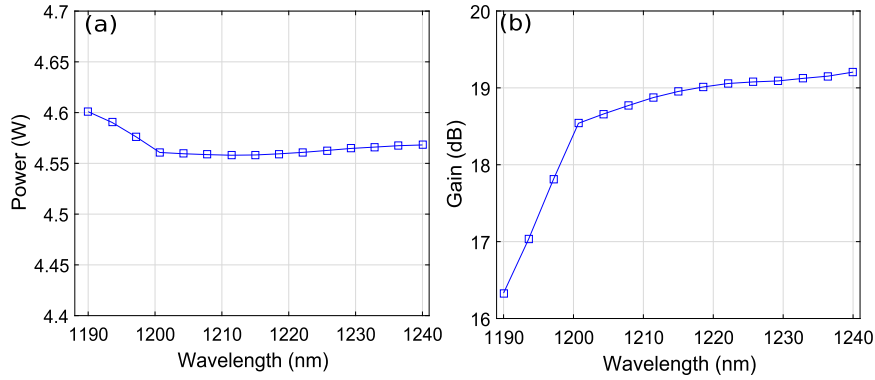**Fig. 7.** Signal wavelength versus (a) gain plot (b) NF plot.

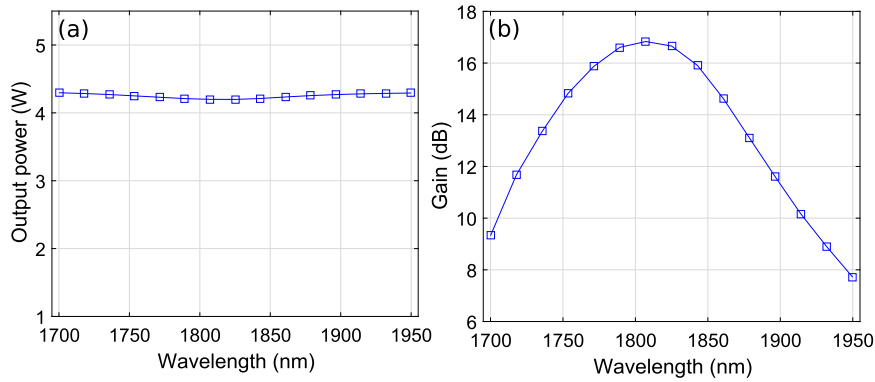**Fig. 8.** Pump wavelength versus (a) Output power plot (b) Gain plot.

Fig. 9. Signal wavelength versus (a) output power plot by considering the PIQ (b) gain plot by considering the PIQ.
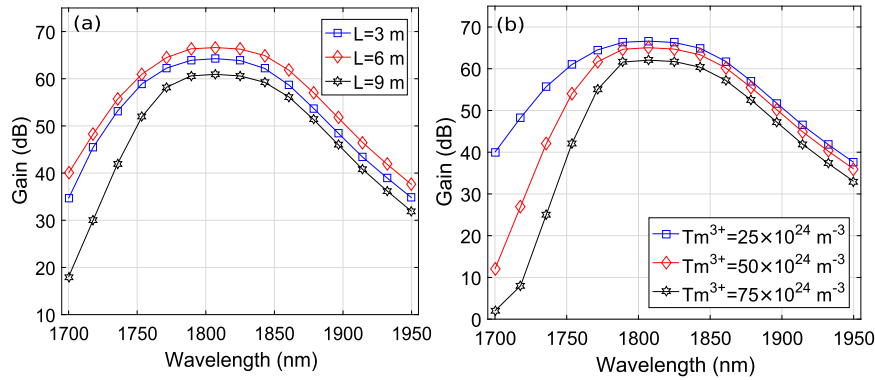

Fig. 10. Signal wavelength versus gain plots as a function of (a) TDF length (b) Tm^{3+} concentration.

powers of 5 W (2.5 W for each pump) and 0 dBm, respectively. The values of cross-relaxation (CR) and homogenous up-conversion (HUC) coefficients used for validation of PIQ are $18 \times 10^{-27} m^3 s^{-1}$ and $0.51 \times 10^{-24} m^3 s^{-1}$, respectively. It may be noticed from Fig. 9a that the output power of the TDFA is decreased by 0.4 W by considering the PIQ. Similarly, it is also evident from Fig. 9b that a penalty of around 2 dB in peak gain of TDFA has been observed at 1807.143 nm by considering the PIQ. Hence, it has been confirmed that the PIQ negatively affects the performance of TDFA by lowering the gain and output power.

6.2. TDFA as in-line Amplifier

The evolution of gain of the TDFA is investigated by varying the wavelength of signal at different TDF lengths and Tm^{3+} concentra-

tions for a signal power of −35 dBm and pump powre of 5 W (2.5 W for each pump) as displayed in Fig. 10. It can be noticed from Fig. 10a that the gain of the TDFA is highest equals to 66.6 dB at 1807.143 nm for TDF length and Tm^{3+} concentration of 12 m (6 m for each TDF) and $25 \times 10^{24} m^{-3}$ for each TDF respectively. Therefore, TDF length of 12 m is turned out as the optimum length yielding the highest gain. It is also evident that the gain gradually decreases after further increasing the length of TDF which is due to a decrease in population inversion [2]. Similarly, the signal wavelength versus gain plots are obtained as a function of Tm^{3+} concentration by considering the optimized TDF length. It is clear that the gain of the TDFA is highest equals to 66.6 dB at Tm^{3+} concentration of $25 \times 10^{24} m^{-3}$ for each TDF as shown in Fig. 10b. Therefore, Tm^{3+} concentration of $25 \times 10^{24} m^{-3}$ is the optimized concentration which yields the highest gain. Fig. 11 shows
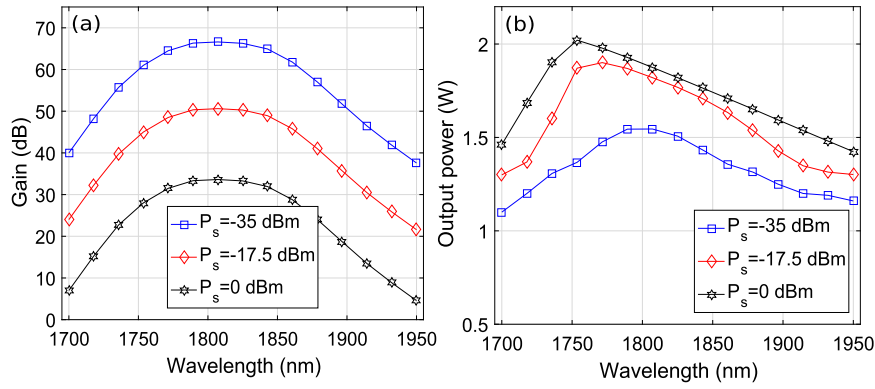
J. Mirza, A. Atieh, M.I. Menhas et al.

Fig. 11. Signal wavelength versus (a) gain plots as a function of signal power (b) output power plots as a function of signal power.
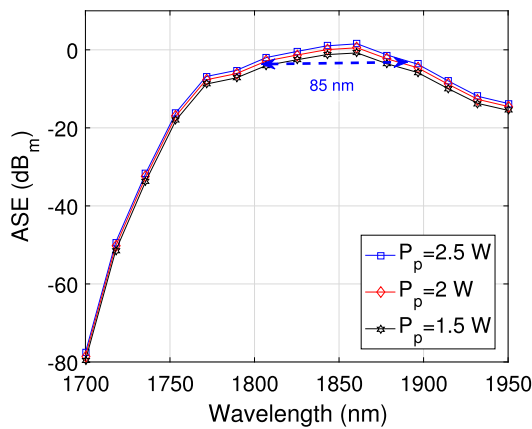

Fig. 12. Signal wavelength versus ASE plots as a function of pump power.

the plots of signal wavelength versus gain and output power as a function of signal power obtained at optimized parameters for pump power of 5 W (2.5 W for each pump). It may be observed from Fig. 11a that the gain of the amplifier is lowest equals to 33.6 dB for signal power of 0 dBm and highest equals to 66.6 dB for signal power of −35 dBm at 1807.143 nm. A decreasing trend in gain of the TDFA is clear for the wavelengths longer than 1810 nm for all signal powers which may be attributed to greater number of Tm^{3+} ions in lower energy manifold than higher energy manifold [2,42]. Similarly, the output power of the amplifier is lowest equals to 1.54 W for signal power of −35 dBm at 1807.143 nm and highest equals to 2 W for signal power of 0 dBm at 1771.429 nm as shown in Fig. 11b. Fig. 12 shows the signal wavelength versus ASE plots obtained at different pump powers at optimized parameters for signal power of −35 dBm. It may be observed that the peak ASE equals to 1.54 dBm is obtained at signal wavelength of 1860.714 nm for pump power of 5 W (2.5 W of each pump). The ASE has a decreasing trend at higher wavelengths which is due to the effect of ground state absorption at higher wavelengths due to poor population inversion [2]. Further, 3 dB ASE bandwidth of 85 nm is obtained for pump power of 5 W.

6.3. System Level Performance of the Designed TDFA

The system level performance of the designed TDFA is investigated for different OWC link ranges versus BER considering strong turbulence regime (i.e. $C_n^2 = 5 \times 10^{-12} m^{-2/3}$) at different values of atmospheric attenuation as shown in Fig. 13. It is important to mention here that the range of first OWC link is kept constant at
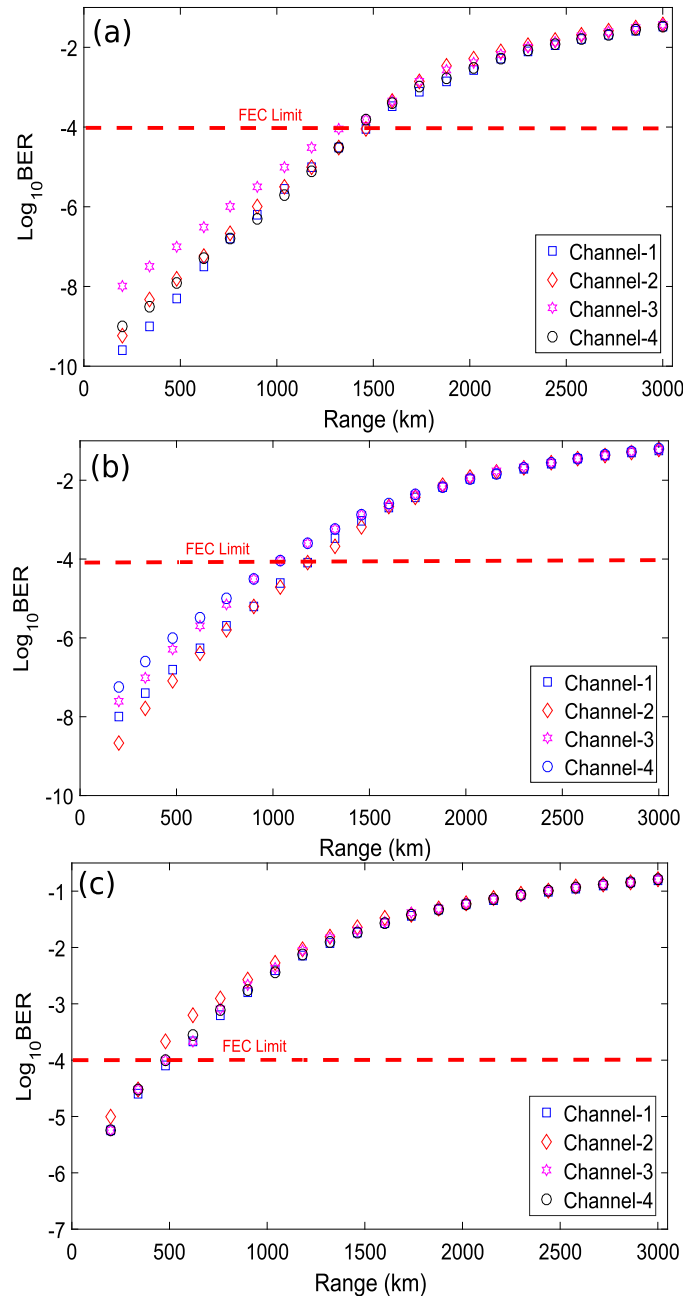

Fig. 13. Range versus BER plots of all four channels obtained at (a) 0.22 dB/m (b) 4 dB/km (c) 5 dB/km.
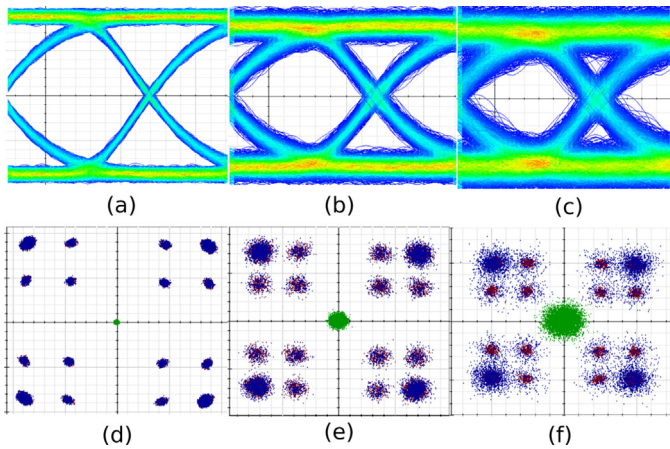
Fig. 14. Eye and constellation plots of channel-1 at (a) and (d) 0.22 dB/km (b) and (e) 4 dB/km (c) and (f) 5 dB/km.

10 km while the range of second OWC link is varied up to 3000 km. The variation in the overall range of OWC link gives different BER values of different channels. It is important to mention here that we are considering FEC limit of 10^{-4}. It may be observed from Fig. 13a that at FEC limit, the maximum error free average range equals to around 1450 km is achieved for all channels at atmospheric attenuation of 0.22 dB/km. At atmospheric attenuation of 4 dB/km, the maximum error free average range equals to around 1100 km is achieved at FEC limit for all channels. Similarly, the maximum error free average range equals to 500 km is achieved for all channels at atmospheric attenuation of 5 dB/km. A small variation in the achieved average range at FEC limit is observed among all four channels at different values of atmospheric attenuation which can be ignored. To further elaborate the performance of the channels, we have obtained the eye diagrams and constellation plots of channel-1 only at FEC limit by considering the strong turbulence and different values of atmospheric attenuation as shown in Fig. 14. Fig. 14a, b, and c show eye diagrams of channel-1 obtained at atmospheric attenuation of 0.22 dB/km, 4 dB/km, and 5 dB/km, respectively. It is clear that the opening of the eye diagrams decreases on increasing the value of atmospheric attenuation. Similarly, Fig. 14d, e, and f show constellation plots of channel-1 obtained at atmospheric attenuation of 0.22 dB/km, 4 dB/km, and 5 dB/km, respectively. We see that the constellations get radiation with increasing values of atmospheric attenuation because of low received optical power at the photodetector. However, the constellations are clearly distant resulting into easy decision at the receiver.

7. Conclusion

The design of an efficient Thulium-doped fiber amplifier for the use as booster as well as in-line based on dual-stage forward pumps for employment in a dual-hop earth to satellite optical wireless Link is proposed. The pumping scheme, length of Thulium-doped fiber, and Tm^{3+} concentration are optimized. Output power of 4.6 W and gain of 18.8 dB are obtained for signal power of 0 dBm at 1807.143 nm when TDFA is considered as booster amplifier while a gain of 66.6 dB and output power of 1.5 W are obtained for signal power of -35 dBm at 1807.143 nm when TDFA is used as in-line amplifier. Noise figure of around 4.4 dB is observed for signal wavelength of 1807.143 nm and power of 0 dBm. The system level performance of the TDFA is evaluated using BER metric for dual-hop earth to satellite OWC link considering Gamma-Gamma channel model at different values of atmospheric

attenuation. The BER results show that different ranges for error free transmission at the FEC limit of 10^{-4} are achieved at different values of atmospheric attenuation.

Declaration of Competing Interest

The authors declare that they have no known competing financial interests or personal relationships that could have appeared to influence the work reported in this paper.

References

[1] WDM Lightwave Systems.: https:// www.fiberoptics4sale.com/blogs/wave-optics/wdm-lightwave-systems; 2021.

[2] Mirza J, Ghafoor S, Habib N, Kanwal F, Qureshi KK. Performance evaluation of Praseodymium doped fiber amplifiers. Opt Rev 2021;28(6):611–8.

[3] Mirza J, Imtiaz WA, Aljohani AJ, Atieh A, Ghafoor S. "Design and analysis of a 32×5 Gbps passive optical network employing FSO based protection at the distribution level. Alexandria Eng J 2020;59(6):4621–31.

[4] Li Z, Heidt AM, Daniel JMO, Jung Y, Alam SU, Richardson DJ. "Thulium-doped fiber amplifier for optical communications at 2 μm. Opt Exp 2013;21 (8):9289–97.

[5] C. Lei, H. Feng, L. Wang, Y. Messaddeq, and S. Larochelle, "An extended L-band EDFA using C-band pump wavelength, In OSA Optical Fiber Communication Conference, pp. W1C–2, 2020.

[6] Donodin A, Dvoyrin V, Manuylovich E, Turitsyn S. Bismuth-doped fibre amplifier operating in E-and S-optical bands. Opt Mater Exp 2020;11 (1):127–35.

[7] A. Napoli, N. Costa, J.K. Fischer, and W. Forysiak, "Towards multiband optical systems," In Photonic Networks and Devices. Optical Society of America, 2018, pp. NeTu3E-1.

[8] Tench RE, Amavigan A, Chen K, Delavaux J-M, Robin T, Cadier B, Laurent A. Experimental performance of a broadband dual-stage 1950 nm PM single-clad Tm-doped fiber amplifier. IEEE Photon Technol Lett 2020;32(15):956–9.

[9] Jackson SD, King TA. High-power diode-cladding-pumped Tm-doped silica fiber laser. Opt Lett 1998;23(18):1462–4.

[10] C. Romano, R.E. Tench, and J-M. Delavaux, "5 W 1952 nm Brillouin-free efficient single clad TDFA, Optical Fiber Technology, vol. 46, pp. 186–191, 201.

[11] Muravyev SV, Anashkina EA, Andrianov AV, Dorofeev VV, Motorin SE, Koptev MY, Kim AV. Dual-band Tm^{3+}-doped tellurite fiber amplifier and laser at 1900 nm and 2300 nm. Scient Rep 2018;8(1):1–13.

[12] C. Gaida, M. Gebhardt, T. Heuermann, Z. Wang, F. Stutzki, C. Jauregui, and J. Limpert, "Ultrafast Tm-doped fiber amplifier with 1 kW average output power, in The European Conference on Lasers and Electro-Optics, Optical Society of America, p. cj_10_4, 2019.

[13] Mukhtar S, Aliyu KN, Magam MG, Qureshi KK. Theoretical analysis of Thulium-doped fiber amplifier based on in-band pumping scheme. Microwave and Optical Technology Letters 2021;63(4):1309–13.

[14] Jin X, Lee E, Luo J, Sun B, Yu X. High-efficiency ultrafast Tm-doped fiber amplifier based on resonant pumping. Opt Lett 2018;43(7):1431–4.

[15] Khamis MA, Ennser K. Study of heavily Thulium-doped fiber amplifier for optical telecom at 2000 nm, in IOP Conference Series. Mater Sci Eng 2019;518 (5):052017.

[16] Khamis MA, Ennser K. "Gain variation induced by power transient in Thulium-doped fiber amplifier at 2μm and its reduction by optical gain clamping technique. Opt Commun 2017;384:89–92.

[17] Li Z, Jung Y, Daniel JMO, Simakov N, Tokurakawa M, Shardlow PC, Jain D. Exploiting the short wavelength gain of silica-based Thulium-doped fiber amplifiers. Opt Lett 2016;41(10):2197–200.

[18] M.A. Khamis, and K. Ennser, "Theoretical model of a Thulium-doped fiber amplifier pumped at 1570 nm and 793 nm in the presence of cross relaxation, Journal of Lightwave Technology, vol. 34, no. 24, pp. 5675–5681, 016.

[19] Y. Jung, Z. Li, N. Simakov, J.M.O. Daniel, D. Jain, P.C. Shardlow, and A.M. Heidt, "Silica-based Thulium doped fiber amplifiers for wavelengths beyond the L-band, in Optical Fiber Communication Conference, Optical Society of America, pp. M3D–5, 2016.

[20] Tench RE, Romano C, Delavaux J-M. "Multistage single clad 2 μm TDFA with a shared L-band pump source. Appl Opt 2018;57(21):5948–55.

[21] Goswami T, Grosek J, Gopalakrishnan J. Simulations of single-and two-tone Tm-doped optical fiber laser amplifiers. Opt Exp 2021;29(8):12599–615.

[22] Singh R, Singh ML. Performance evaluation of S-band Thulium doped silica fiber amplifier employing multiple pumping schemes. Optik 2017;140:565–70.

[23] Tench RE, Romano C, Delavaux J-M. "Broadband 2 W Output Power Tandem Thulium-Doped Single Clad Fiber Amplifier at 2μm. IEEE Photon Technol Lett 2018;30(5):503–6.

[24] Tench RE, Amavigan A, Romano C, Traore D, Delavaux J-M, Robin T, Cadier B, Laurent A, Crochet P. 3.5 W broadband PM hybrid amplifier at 2051 nm with Holmium-and Thulium-doped single-clad fibers. J Lightwave Technol 2021;39 (5):1471–6.

[25] Tench RE, Romano C, Delavaux J-M. 25 W 2 μm broadband polarization-maintaining hybrid Ho-and Tm-doped fiber amplifier. Appl Opt 2019;58(15):4170–5.

[26] OptiSystem Overview: https://optiwave.com/optisystem-overview/.

[27] Zheng Z, Hua N, Zhong Z, Li J, Li Y, Zheng X. Time-sliced flexible resource allocation for optical low earth orbit satellite networks. IEEE Access 2019;7:56753–9.

[28] Arienzo L. Green RF/FSO communications in cognitive relay-based space information networks for maritime surveillance. IEEE Trans Cognit Commun Network 2019;5(4):1182–93.

[29] Kaushal H, Kaddoum G. Optical communication in space: Challenges and mitigation techniques. IEEE Commun Surv Tutor 2016;19(1):57–96.

[30] Mirza J, Imtiaz WA, Aljohani AJ, Ghafoor S. A high bit rate free space optics based ring topology having carrier-less nodes. IET Commun 2021;15(11):1530–8.

[31] Mirza J, Ghafoor S, Ahmad W, Salman A, Qureshi KK. Integrating ultra-wideband and free space optical communication for realizing a secure and high-throughput body area network architecture based on optical code division multiple access. Opt Rev 2021;28(5):525–37.

[32] S.A. Al-Gailani, M.F. Mohd Salleh, A.A. Salem, R.Q. Shaddad, U.U. Sheikh, and T.A. Almohamad, "A survey of free space optics (FSO) communication systems, links, and networks, IEEE Access, vol. 9, pp. 7353-7373, 2020.

[33] Mirza J, Aljohani AJ, Raza A, Iqbal S, Ghafoor S. A multi-hop free space optical link based on a regenerative relay. Alexandria Eng J 2022;61(2):1459–67.

[34] D.I. Franz Fidler, "Optical communications from high-altitude platform stations, Ph.D dissertation, 2007.

[35] Husein AHM, El-Nahal FI. "Optimizing the Thulium doped fiber amplifier (TDFA) gain and noise figure for S-band 16×10 Gb/s WDM systems. Optik 2013;124(19):4052–7.

[36] Mirza J, Ghafoor S, Kousar A, Kanwal B, Qureshi KK. Design of a Continuous-Wave Ytterbium-Doped Tunable Fiber Laser Pump for Thulium-Doped Fiber Amplifiers. Arab J Sci Eng 2022;47(3):3541–9.

[37] Arnon S. Performance of a laser satellite network with an optical preamplifier. J Opt Soc Am A 2005;22(4):708–15.

[38] Mirza J, Ghafoor S, Hussain A. All-optical generation and transmission of multiple ultrawideband signals over free space optical link. Opt Eng 2019;58(5):056103–8.

[39] Technical specifications of FSO telescopes.: http://www.fsona.com/product.php?sec=10000ep.

[40] Technical specifications of TDF.: https://www.ixblue.com/wp-content/uploads/2021/12/ixbluephotonicstmhotmhodopedfibers.pdf.

[41] Amin MZ, Qureshi KK, Hossain MM. Doping radius effects on an erbium-doped fiber amplifier. Chin Opt Lett 2019;17(1):010602.

[42] Sani M, Aliyu KN, Qureshi KK. Performance evaluation of Er^{3+}/Yb^{3+} codoped fiber amplifier. Microwave Opt Technol Lett 2020;62(6):2243–7.

Khurram Karim Qureshi (SM'12) received a BSc degree with honors in Electrical Engineering from the University of Engineering and Technology (UET), Lahore, Pakistan, and a Ph.D. also in Electrical Engineering from the Hong Kong Polytechnic University in 2006. He is currently a Professor with the Electrical Engineering Department of King Fahd University of Petroleum and Minerals (KFUPM). His research interests include optical communications, optical signal processing, lasers, sensors, and miniaturized antennas. He is a senior member of IEEE, USA, and has published more than 90 journal and conference papers, and five US patents issued to his credit.